

Article

# Wet-Deposited TADF-Based OLED Active Layers: New Approaches towards Further Optimization

Francisco Teixeira, José Carlos Germino  and Luiz Pereira \* 

Department of Physics and i3N—Institute for Nanostructures, Nanomodelling and Nanofabrication, University of Aveiro, 3810-193 Aveiro, Portugal; franciscomteixeira@ua.pt (F.T.); germino@ua.pt (J.C.G.)

\* Correspondence: luiz@ua.pt

**Featured Application:** A basic framework for further large-area OLEDs via printed electronics.

**Abstract:** The effects of the solvent used for the active layer materials of an OLED based on TADF emitters play a fundamental role in solution-deposited devices. This work focuses on the effects on the performance of different solvents employed to fabricate a very simple two-organic-layer OLED based on a green TADF emitter, under the concept of host: guest matrix. From the different results of the main figures of merit, it was possible to conclude that the OLED that used toluene as a solvent for the active layer reached a maximum EQE of 14%, almost the maximum already obtained for this emitter in more complex device structures. With the analysis of the charge-transport processes, it was possible to establish an explanatory model for the obtained results. Through impedance spectroscopy, additional characterization of the nature of charge-transport processes was carried out. With these results, it was possible to correlate the relaxation times, with the electrical properties of the active layer, and make inferences about the interaction between the electrical charges and the defect levels, opening new possibilities for further development in printed OLEDs.

**Keywords:** solution-deposited OLEDs; TADF; device structural defects; OLEDs charge balance; efficient OLED simple structure



**Citation:** Teixeira, F.; Germino, J.C.; Pereira, L. Wet-Deposited TADF-Based OLED Active Layers: New Approaches towards Further Optimization. *Appl. Sci.* **2023**, *13*, 12020. <https://doi.org/10.3390/app132112020>

Academic Editor: John Xiupu Zhang

Received: 26 September 2023

Revised: 22 October 2023

Accepted: 25 October 2023

Published: 3 November 2023



**Copyright:** © 2023 by the authors. Licensee MDPI, Basel, Switzerland. This article is an open access article distributed under the terms and conditions of the Creative Commons Attribution (CC BY) license (<https://creativecommons.org/licenses/by/4.0/>).

## 1. Introduction

Organic light-emitting diodes (OLEDs) play an important role in display technology nowadays and have started to become an important field of research for lighting. Since Tang's and VanSlyke's pioneer work [1] in a thermal evaporated double-organic-layer device, composed of tris(8-hydroxyquinolate)aluminum(III) (electron transport and emissive layer—ETL and EML, respectively) and an aromatic diamine (hole transport layer—HTL), fast growth of the academical and industrial research has been noted due to the possibility of obtaining a practical and feasible device [2]. OLED research can be divided into five main technologies: first—fluorescent emitters [3]; second—phosphorescent emitters [4]; third—thermally activated delayed fluorescent (TADF) emitters [5–7]; fourth—hyperfluorescent emitters [8]; and, most recently, fifth—usage of nonresonant energy transfer process to pump up OLEDs efficiency [9,10]. Also, solution-processable protocols (i.e., spin-coating [11], blade coating [12], inkjet [13], screen printing [12], and slot-die coating [14]) have been adopted to achieve easy up-scaling devices, coupled with urgent cost-, energy-, and material-saving demands [15].

In particular, TADF dyes have played an important role in highly efficient OLEDs' emissive layers (EMLs) due to their ability to ease optoelectronic feature tunability via simple chemical structure modifications [16,17]. Such an advantage enables the achievement of external quantum efficiencies (EQEs) up to the theoretical limit for a simple architecture device, and in a wide gamma of emitting colors at the entire visible spectrum [18–22]. As usual, TADF molecules are composed of an electron donor (D) and acceptor (A) moieties

chemically bonded, which is capable of creating a charge-transfer (CT) state, and, with an orthogonal orientation between D and A parts, it can create a small energy barrier between the first excited singlet and triplet states ( $\Delta E_{ST} \approx 0$ ) [23]. When these organic dyes have those characteristics, they can undergo a thermally activated reverse inter-system crossing (rISC), enabling TADF emitters to theoretically achieve internal quantum efficiencies (IQE) of 100%, according to the singlet/triplet spin statistics [23,24]. However, TADF molecules present strong triplet–triplet annihilation (TTA) pathways and sensitivity to the local chemical environment (solvatochromism) due to their active triplet states involved in the delayed fluorescence electronic structure reorganization [25–29]. Those characteristics imply that the use of TADF molecules for OLED's EML can only be made in a host: guest system at small concentrations, diminishing emitting losses via a nonradiative recombination process. Globally, a compromise between an efficient TADF process and the final device figures of merit must be considered for their emitting diodes [30,31].

The OLED fabrication techniques were almost based on thermal evaporation methods as they can, in a well-controlled process, give highly efficient and reliable devices (due to the best molecular conformation of the deposited layers, specifically those containing small molecules). The focus is, naturally, displays. To achieve an optimum electrical charge balance and confine the exciton recombination region in the emissive layer, a complex OLED structure needs to be made. Additionally, for efficient emitters (transition metals complexes and TADFs), the abovementioned emission quenching implies the use of a co-evaporation process to achieve the host: guest concept, avoiding quenching and promoting an efficient energy transfer from host to guest (emitter). In the end, efficient OLEDs made by thermal evaporation process are particularly expensive and the process is prone to faults as the masks can be minimally misaligned. Despite such issues, thermal evaporated OLEDs are still the industry standard for displays.

A completely different framework has to be created towards a low-cost fabrication technique. As the demand for OLEDs increases, the industry needs to move towards a new deposition process, as the complex and expensive thermal evaporation does not appear to be a solution; moreover, it is not compatible with the everyday more important concept of printed electronics, where the fabrication process is simple, low-cost, and with high-output production [32]. However, despite the first results, which indicate the easy possibility of producing reliable OLEDs by solution depositions, the overall figures of merit are poor. Those wet deposition methods are prone to increasing structural defects in the organic layers, some of them electrically active with a strong influence on trapping/detrapping of the electrical carriers, with an impact on the electrical balance efficiency [33,34]. On other hand, the simplification of the device structure was achieved. The current main efforts are focused on the deposition parameters/procedures to obtain more “trap-free” organic layers (best molecular conformation) and in the host: guest optimal composition to promote the best energy transfer process and exciton recombination. The final goal is to achieve the best trade-off between efficiency and a low-cost simple OLED structure. Among the several OLED solution-deposition processes, spin-coating is one of the most interesting for research development. The choice of spin-coating for the deposition relies on the technique's simplicity and well-known good film formation in small-area emitters [35].

Several works in recent years show that this objective is possible, although the best results depend on a more complex structure [36–42]. As reported in several of those works, we need to play (besides the organic materials) with the solvents, concentrations, and deposition parameters as the fundamental keys [43].

In recent years, Pereira and his co-workers [44–48] have carried out comprehensive studies about how to optimize electrical and morphological properties of solution-processable mixed-host layers for efficient TADF OLEDs based on simple architectures. These mixed-host layers are composed of poly(9-vinylcabazole) (PVK) (a well-known transparent p-type polymer) and an ambipolar, p-type or n-type semiconductive small molecule for obtaining a balance of charge-carrier and density of injected electrons and holes into the EML. The electrical and morphological optimization of such kinds of layers enables

the achievement of highly efficient solution-processable TADF OLEDs (EQEs beyond 15%) [45,46]. In particular, a PVK:OXD-7 (1,3-bis[2-(4-*tert*-butylphenyl)-1,3,4-oxadiazole-5-yl]benzene) mixed host with 2PXZ-OXD (2,5-bis(4-(10H-phenoxazin-10-yl)phenyl)-1,3,4-oxadiazole) green-emitter TADF guest enabled Pereira's group to achieve EQE up to 10% in a unique organic layer OLED, the best result for this material in such a type of simple architecture [44]. Moreover, this TADF emitter, as the previous works have carried out (and shown in the related references cited here) is particularly complicated to be used as an emitter, as the interactions with the organic environment induce a complex energy transfer process that results in an emission loss. Therefore, it is a challenge to develop and optimize a solution-deposited OLED, in a simple structure, that uses this TADF as an emitter. Nonetheless, a comprehensive study about how different solvents with specific physical–chemical properties and interactions must be performed to better understand the local chemical environment's influence on the OLED's morphological, electrical, and optical features.

In this sense, herein, we exploit a detailed study about how four different solvents for processing OLED's EML, composed of PVK, 1,3-Bis(N-carbazolyl)benzene (mCP) (ambipolar semiconducting small molecule) and 2PXZ-OXD, change their optoelectronic properties in solution-processed OLEDs by spin-coating technique. Toluene (Tol), chlorobenzene (CB), chloroform (CHCl<sub>3</sub>), and tetrahydrofuran (THF) were selected considering differences in their physical–chemical properties (vapor pressure, boiling point, viscosity, density, dielectric constant, among others) and specific chemical interactions with the EML solutes to understand their impact on the electrical and optical properties of OLEDs. Electroluminescent devices were assembled following the straightforward architecture: ITO | PEDOT:PSS | EML | TPBi | LiF | Al. Electroluminescence (EL) spectra reveal a considerable redshift in the emission bands, according to the solvent polarity, vapor pressure, and boiling point, as well as specific molecular interactions: high polarity, vapor pressure, and boiling solvents (i.e., THF and CHCl<sub>3</sub>) present EL maxima band close to 525 nm, while CB and Tol solvents have EL close to 495 nm; an effect probably linked to the fast evaporation of THF and CHCl<sub>3</sub> solvents in contrast to other ones during the thermal annealing of the active layer. Also, the THF solvent could have strong chemical interactions with the EML molecules, which, combined with its high vapor pressure, can create more crystalline domains, making it able to form molecular aggregates that have low-energetic emissive states. Those different solvents also directly impact the OLED's figures of merit (FOM, particularly luminance (L), external quantum efficiency (EQE), power efficiency ( $\eta_p$ ), and current efficiency ( $\eta_c$ )), achieving the best results for Tol:  $V_{on} = 4.0$  V,  $L_{max} = 3270$  cd m<sup>-2</sup>,  $EQE_{max} = 14\%$ ,  $\eta_c = 24.3$  cd A<sup>-1</sup>, and  $\eta_p = 16.9$  lm W<sup>-1</sup>; small efficiency losses (roll-off) until 1000 cd m<sup>-2</sup> for all solvents (32%, 6%, 1%, and 25% for Tol, CB, CHCl<sub>3</sub>, and THF, respectively). To better understand those features, DC and AC electrical measurements in ambipolar and only-hole and -electron devices were employed considering space-charge-limited current models (SCLC) and impedance spectroscopy, respectively. Finally, this work reveals that different chosen solvents have a strong impact on the 2PXZ-OXD TADF solution-processed OLEDs, even after thermal treatment of the active layer, regarding efficiency losses and EL emission energies, opening doors for a wide range of fundamental chemical interactions (i.e., Raman, NMR, FTIR, photophysical, and time-resolved spectroscopies), structural (small-angle and grazing incidence X-ray scattering–SAXS and GIWAXS, respectively), and morphological studies on mixed hosts for highly efficient solution-processable TADF OLEDs.

## 2. Materials and Methods

### 2.1. Materials

Poly(ethylenedioxythiophene):poly(4-styrenesulfonate) (PEDOT:PSS) and patterned ITO-glass substrates were purchased from Ossila company. 2,2',2''-(1,3,5-Benzinetriyl)-tris(1-phenyl-1-H-benzimidazole) (TPBi) and 2,5-bis(4-(10H-phenoxazin-10-yl)phenyl)-1,3,4-oxadiazole (2PXZ-OXD) were purchased from Lumtech Ltd., Taiwan. Poly(9-vinylcarbazole)

(PVK; MW = 1,100,000 g mol<sup>-1</sup>), 1,3-Bis(N-carbazolyl)benzene (mCP), lithium fluoride (LiF; 99.999%), Hellmanex<sup>®</sup>, toluene, chlorobenzene, chloroform, and tetrahydrofuran (anhydrous and inhibitor-free grade solvents) were purchased from Sigma-Aldrich, Portugal. All chemicals were used without further purification. Figure 1 shows the simple molecular scheme of the materials employed in this work.

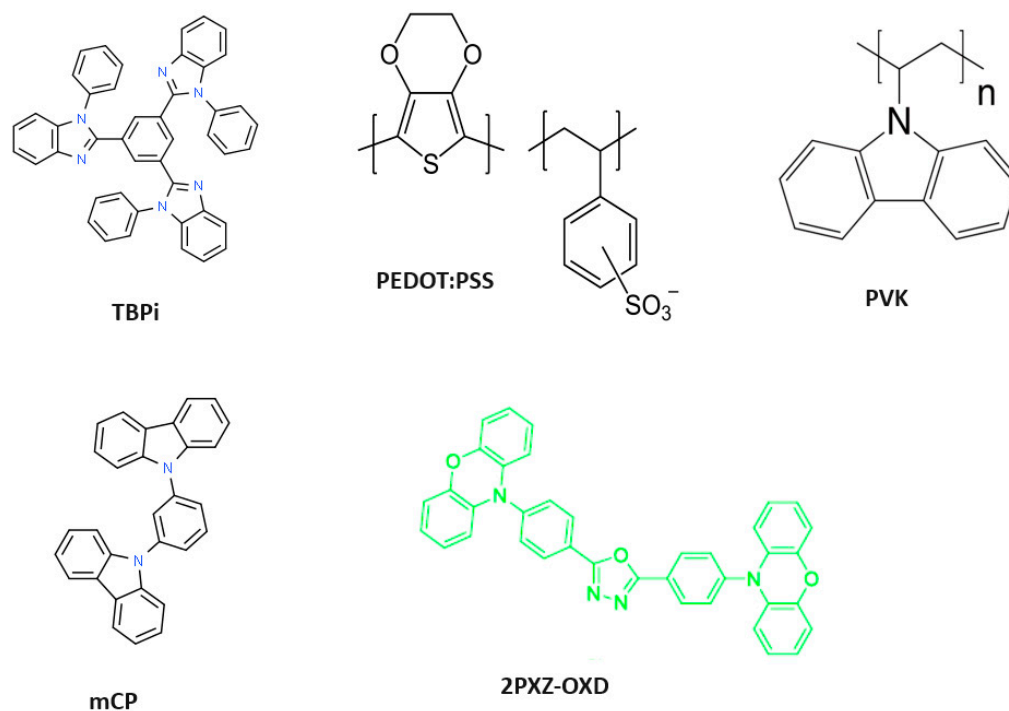


**Figure 1.** Molecular structures of TPBi, PEDOT:PSS, PVK, mCP and 2PXZ-OXD.

## 2.2. Photophysical Measurements

Electronic absorption spectroscopy was acquired using a Shimadzu UV-Vis UV-2100. Photoluminescence (PL) and PL excitation (PLE) spectroscopies measurements were obtained from a Fluorolog-3 Horiba Scientific set-up fluorimeter, using excitation and emission wavelengths at 290 nm and 500 nm, respectively.

## 2.3. OLEDs Fabrication and Single Carrier Devices

ITO-glass substrates were cleaned under sonication, using 2% Hellmanex<sup>®</sup> solution for 30 min. Substrates were washed subsequently with hot water, acetone, and IPA for 15 min for each step in a heated ultrasonic bath. Then, substrates were treated with NaOH 10%vol under sonication for 5 min, rigorously washed with deionized hot water, and dried with N<sub>2</sub>(g) jet. PEDOT:PSS (30 nm) were dynamically deposited by spin-coating technique (5000 rpm; 30 s), and films were annealed in a controlled oven at 120 °C for 10 min. Then, PEDOT:PSS deposited films were transferred to an N<sub>2</sub>(g) controlled atmosphere MBraun Glovebox ([O<sub>2</sub>] < 10 ppm; [H<sub>2</sub>O] < 0.1 ppm), where the solutions of 2PXZ-OXD (10%wt) into PVK:mCP (3:2; 10 mg mL<sup>-1</sup>; ~50 nm) of each solvent were spin-casted as EML. Finally, TPBi (40 nm; ETL), LiF (0.5 nm; EIL), and Al (80 nm) electrical contact were thermally evaporated under ultra-vacuum conditions ( $p < 5 \times 10^{-6}$  mbar), obtaining OLEDs with the following configuration: ITO | PEDOT:PSS | PVK:mCP:2PXZ-OXD | TPBi | LiF | Al. It should be noted that the ITO | PEDOT:PSS “layer” is considered an optimized anode (work function near 5.2 eV, as widely reported in the literature [47]), and due to the “metal-like” behavior of PEDOT:PSS we will not take it into account for the total “pure” organic layers) and, oppositely, the LiF | Al “layer” is an optimized cathode (accepted work function near 3 eV [47]), mainly due to the well-known quantum tunneling effect through dielectric LiF material. In such a framework, we will consider (as usual) that our devices are made with

only two “pure” organic layers (from an electrical point of view). The final active area of each OLED was 4.5 mm<sup>2</sup>.

Single-carrier diodes were assembled with the following architecture: ITO | PEDOT:PSS | PVK:mCP:2PXZ-OXD | PEDOT:PSS | Al and ITO | LiF | PVK:mCP:2PXZ-OXD | LiF | Al for the only-hole and -electron transport, respectively. Conditions of the film deposition, thermal evaporation of LiF and Al, and the J–V measurements were the same as the ones used for the OLEDs. The simple energy band diagram (with optimized anode/cathode work functions and pure organic HOMO/LUMO levels) is shown in Figure 2.

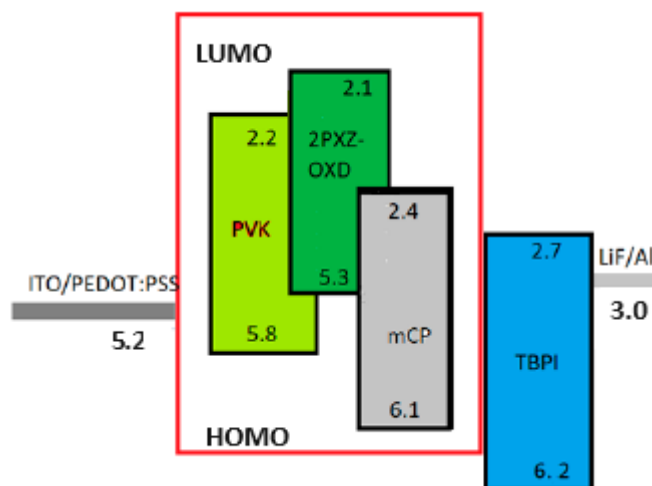


**Figure 2.** Device energy levels. The red line shows the active layer with the organic materials of the host (PVK and mCP) and guest (2PXZ-OXD) in the matrix. All values are in eV.

#### 2.4. Devices Opto-Electrical Characterization

The electroluminescent OLEDs current and luminance versus voltage curves (J,L–V) were measured using a Keithley 2425 source meter unit and a Konica Minolta CS110 Luminance Meter coupled to a close-up lens No. 110,  $\phi = 40.5$  mm, 20–30 cm, in a proper OLEDs sample holder. EL spectra were acquired using a USB4000 Ocean Optics CCD spectrometer. Luminance and EL measurements were obtained from the normal angle concerning the samples. All OLED figures of merit (current efficiency— $\eta_C$ , power efficiency— $\eta_P$ , and external quantum efficiency—EQE) were calculated considering Lambertian emission from devices. Impedance spectroscopy measurements were made using a Fluke PM6306 programmable RCL-meter with an AC level of 0.1 V, an internal bias of 0 V, and frequencies from 100 Hz to 1 MHz. All measurements were made at room temperature.

### 3. Results and Discussion

#### 3.1. Basic Photophysical Characterization

A steady-state photophysical study was carried out to help to understand the active layer material solvent effect in the active layer, evaluating the TADF behavior in a matrix of PVK:mCP. PLE (photoluminescence excited—Figure 3a) spectrum of the film was obtained with an excitation energy corresponding to the photoluminescent (PL) main peak. After the absorption, the excited electrical carriers will relax to an intermediary lower energy state, with a nonradiative transition followed by a photon emission (with lower energy than the absorbed one) to the ground state. The PL spectra of each sample were obtained by using an excitation wavelength of  $\lambda_{exc} = 290$  nm with the correspondent filter (WG295) to eliminate Rayleigh scattering from the source. This specific  $\lambda_{exc}$  can electronically excite the host matrix (PVK:mCP) in contrast to the TADF molecule [49]. Such a strategy is important to evaluate the possible presence of radiative and nonradiative energy transfer processes (trivial and resonant mechanisms, respectively) from the host to the guest molecules. This important feature might impact the OLEDs’ EML efficiency. The nonradiative processes

are mainly governed by Forster and Dexter mechanisms, depending only on the excited-state dipole orientation, the spectral overlap of emission and absorption spectra, and the distance between the donor (host) and acceptor (guest) molecules [50]. In addition to the predominance of the CT PL band of TADF in the PL spectra of solution-processed EML for different solvents (Figure 3b), only a small contribution of the host emission (inset Figure 3b), even electronically exciting the host matrix, can be observed. We can see clear evidence of the predominant nonradiative (resonant) energy transfer (RET) process from the PVK:mCP to the 2PXZ-OXD. Looking at the PLE spectra (Figure 3a) monitoring the TADF emission band (500 nm), we can prove the presence of such an RET process among host–guest systems in the EML. We observe the characteristic CT excitation band of 2PXZ-OXD molecules around 400 nm with a minimal intensity when compared to the excitation bands of the PVK polymer:  $\lambda_{exc} = 341$  nm, 328 nm, and 294 nm, which is assigned to the  $S_0 \rightarrow S_1$ ,  $S_0 \rightarrow S_2$ , and  $S_0 \rightarrow S_3$  PVK singlet electronic transitions [51]. These observations, although not completely assertive, are good evidence that our active layers are well organized morphologically at the molecular level. The very small redshift in the PL spectrum (around 8 nm) seems to be not significant so it is considered that the use of different solvents will not have an impact on the energy transfer process.

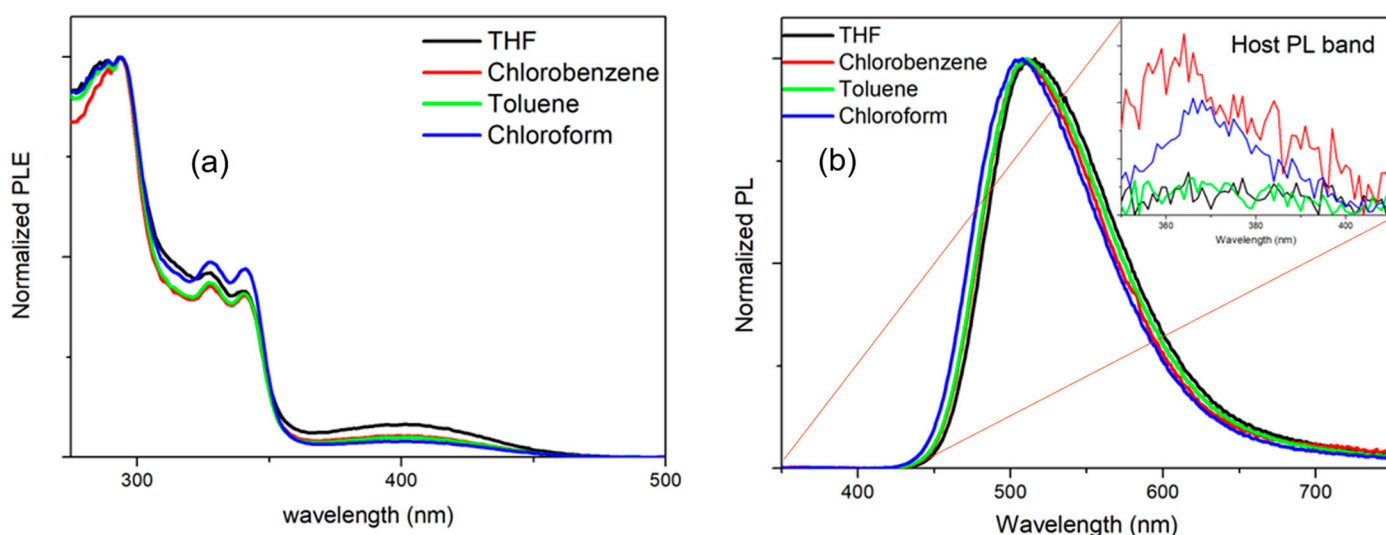


**Figure 3.** (a) PLE spectrum for each kind of device obtained with the excitation wavelength corresponding to the central maximum of photoluminescence spectrum. (b) Photoluminescence spectrum (inset: the small emission of the host material).

### 3.2. Electrical Behavior: Current Density–Applied Voltage–Brightness and Efficiencies

The J–V–L data for all kinds of samples are shown in Figure 4. From the J–V–L data, it is possible to see that all devices showed a very low turn-on voltage ( $V_{on}$ ), between 4 and 5 V, a remarkable performance for a simple two-organic-layer structure. The devices that used THF as a solvent for the active layer materials showed one of the best results (on average). The maximum brightness was about  $4030 \text{ cd m}^{-2}$ , the maximum EQE was 10.5%, the  $\eta_{C_{max}}$  was  $20.0 \text{ cd A}^{-1}$ , and the  $\eta_{P_{max}}$  was  $8.7 \text{ lm W}^{-1}$ . The devices (again, on average) with the best results were the ones that used toluene as a solvent for the active layer materials. This showed a maximum brightness of  $3240 \text{ cd m}^{-2}$ , a  $\eta_{C_{max}}$  of  $24.3 \text{ cd A}^{-1}$ ,  $\eta_{P_{max}}$  of  $16.9 \text{ lm W}^{-1}$ , and a maximum EQE of 14%; this efficiency is very good and is very close to the best in the literature [52], corresponding to a fully evaporated device with a complex structure of four/five organic layers. Looking at these results, it is possible to see that the device that used toluene as a solvent for the active layer showed the lowest  $V_{on}$  and the best equilibrium between the current efficiency and the power efficiency. This equilibrium results in an EQE value good enough for this type of device structure.

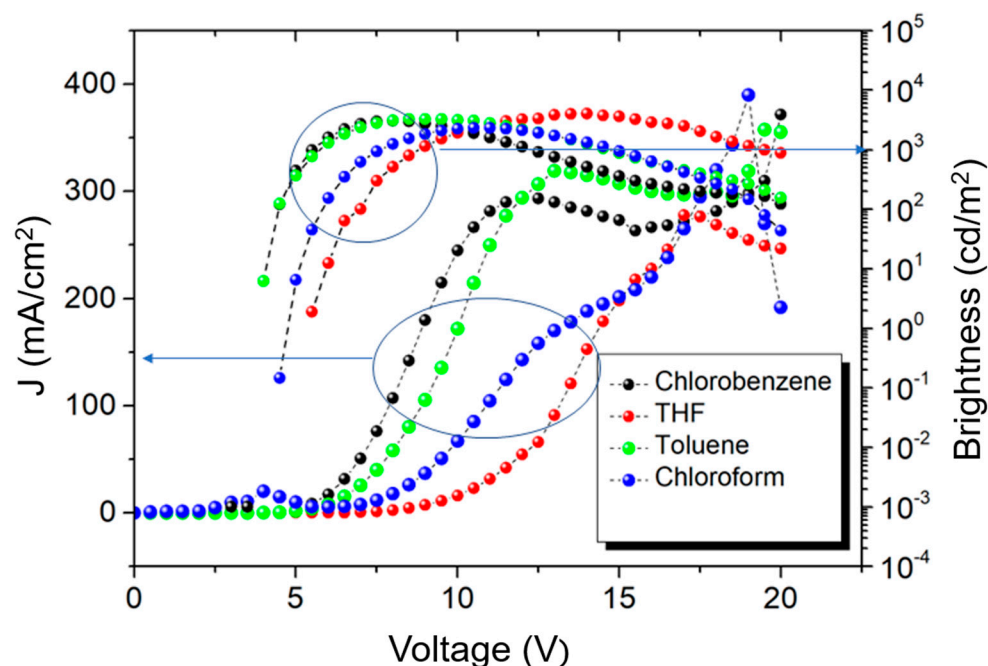


**Figure 4.** Current density and brightness as a function of the applied potential for every kind of OLED made with the different solvents for the active layer.

In opposition, the device that used chloroform as a solvent for the active layer showed a current efficiency of only  $3.7 \text{ cd A}^{-1}$ , a power efficiency of  $7.9 \text{ lm W}^{-1}$ , a maximum brightness of  $2330 \text{ cd m}^{-2}$ , and a  $V_{\text{on}}$  of 5 V. This device showed the lowest maximum EQE about 5.5%. The overall efficiency data are shown in Figure 5.

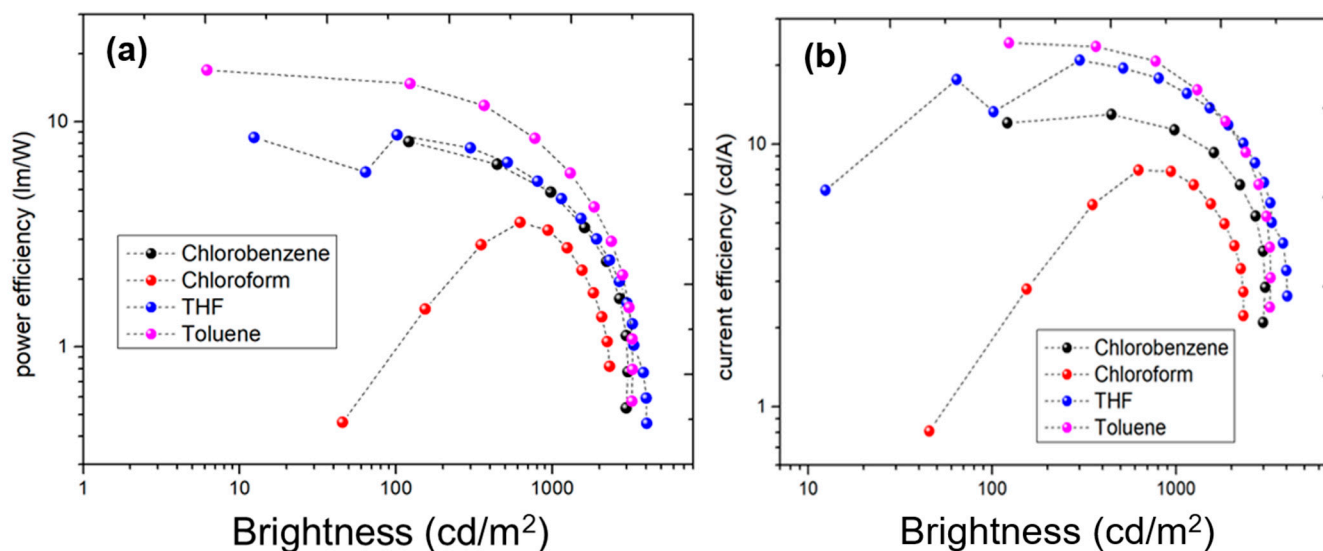


**Figure 5.** (a) Plot of power efficiency and (b) plot of current efficiency as a function of the brightness for every OLED made with the different solvents for the active layer. The fast decrease observed for brightness higher than  $\approx 2000 \text{ cd m}^{-2}$  is due to the device's irreversible degradation.

Finally, in Figure 6, comparative data for the EQE are shown (also as a dependence on brightness). It should be noted that, instead of the usual behavior of the simple solution-deposited OLED device structure, we achieved a particularly interesting low roll-off) when we analyzed the EQE at maximum brightness and at  $1000 \text{ cd cm}^{-1}$ . The lower roll-off appeared in the device that used chloroform as a solvent for the active layer, about 1%. The device that used toluene as a solvent for the active layer materials was the one that

showed the worst roll-off, about 32%. In the bright region analyzed, the OLED where we used THF as solvent for the active layer materials showed a roll-off of 25% and the device where we used chlorobenzene as solvent for the active layer materials showed a roll-off of 6%. With these results, we can observe that until  $1000 \text{ cd m}^{-2}$  these devices are very stable, and we are not employing and blocking layers. These values also show that the device can support the increase in the applied voltage, reaching high brightness values with stability. Moreover, compared with some performances reported in the literature, based on such TADF emitters but with a much more complex structure (and with organic layers thermally evaporated, decreasing the structural defects formed), we are running at the edge as much as possible. A deeper discussion will be provided further ahead.

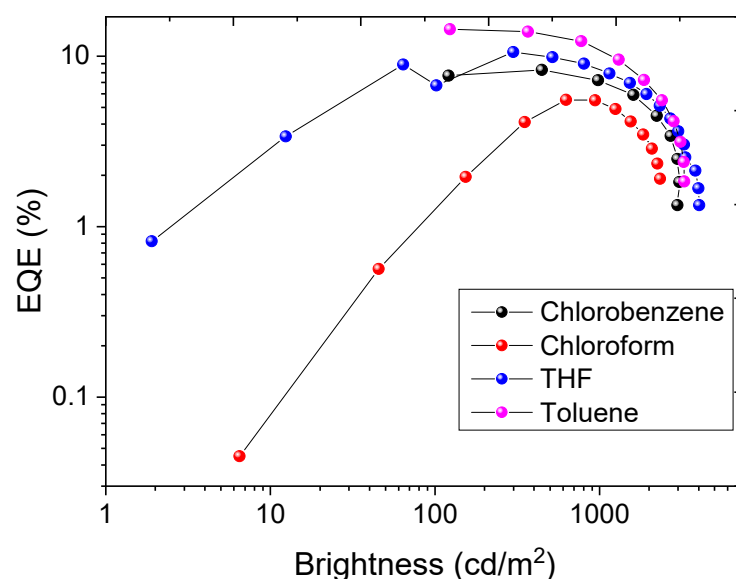


**Figure 6.** EQE as a function of the brightness of the devices.

### 3.3. Electroluminescence and Color Coordinates

The electroluminescence (EL) spectrum for the OLEDs made with different solvents for the active layer is shown in Figure 7. It is possible to see the existence of two peaks for the devices made using the THF and chloroform as solvent and three peaks for chlorobenzene and toluene. The first peak that appears in the spectrum for the chlorobenzene and toluene, at about 380 nm, corresponds to the well-known PVK emission [53,54], which causes a blue shift in the device emission with these solvents. The origin of this peak is related to the incomplete charge transferred from PVK to 2PXZ-OXD. Since this spectrum was taken at 10 V, the electrical charge density is particularly high in the active layer and PVK starts to emit.

The spectrum where THF was employed as solvent shows a central peak at 525 nm and a secondary peak at 492 nm. For the chlorobenzene, the principal peak appears at 499 nm and the secondary peak appears at 532 nm; this indicates that there exists a blueshift when this solvent was used, which is provoked by the PVK emission. For toluene, the spectrum shows a central peak at 498 nm and a secondary peak at 520 nm. Lastly, the spectrum obtained when chloroform was used as a solvent has two very close peaks; the first and principal peak appears at 507 nm and the secondary peak appears at 526 nm. The principal peak in these spectra corresponds to the TADF emission. The secondary peak is associated with a nonplanar vibration that happens in the oxazole group [55]. With the data obtained, it is possible to see that the use of different solvents changes the EL emission. This shift also indicates that the solvent will act in the recombination and charge-transport mechanisms.

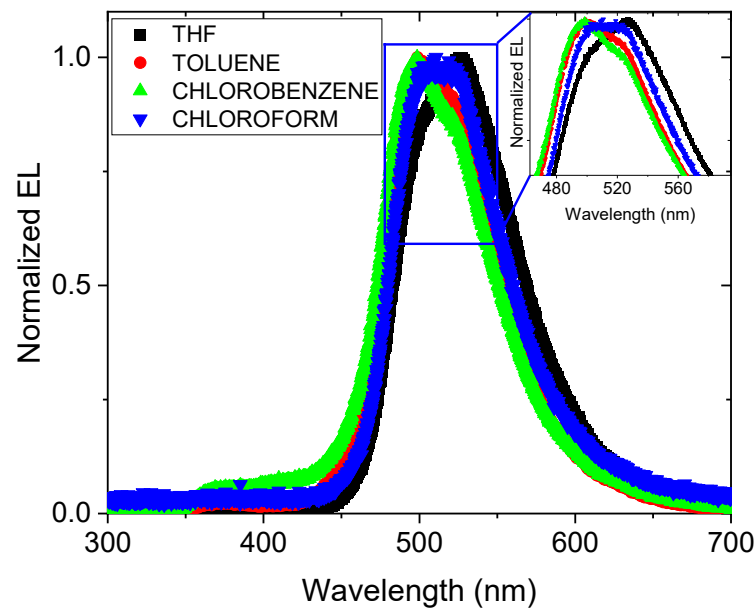


**Figure 7.** Electroluminescence spectra obtained for an applied voltage of 10 V for every OLED made with the different solvents for the active layer.

In Figure 8, it is possible to see the color coordinates for every OLED with different solvents that were used in the active layer.

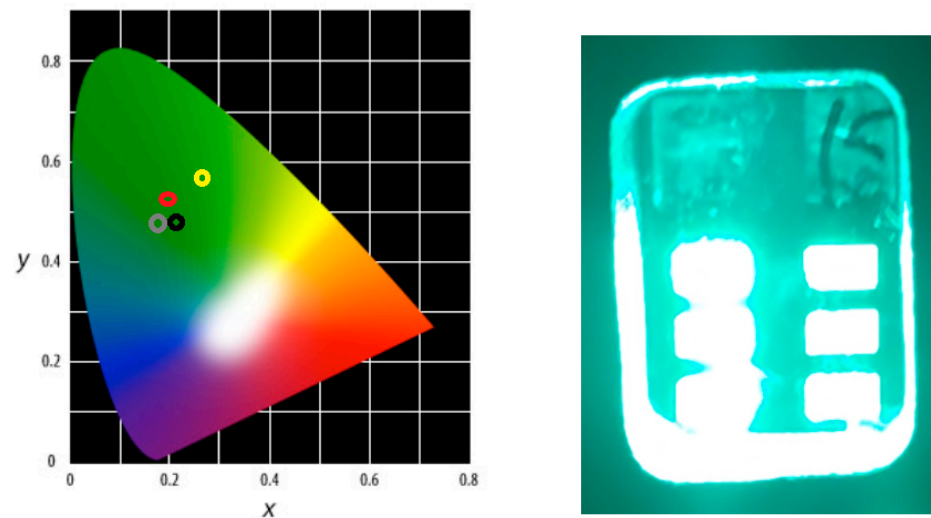


**Figure 8.** CIE chromaticity diagram with the color coordinates for every OLED made with the different solvents for the active layer. The correspondent color coordinates are (0.23; 0.47) for chloroform (black points), (0.28; 0.57) for THF (yellow point), (0.22; 0.50) for toluene (red points), and (0.22; 0.47) for chlorobenzene (grey point). Photo is of an OLED working at 10 V.

Joining the CIE color coordinates information with the EQE behavior (with brightness), it is naturally observed that the different solvents provoke changes in the color coordinates. If we move from THF to chlorobenzene and chloroform, it is possible to see that there exists a blueshift in the color coordinates. This can be an indication that the different solvents will make different changes in the molecular conformation. These modifications can be an indication that the use of different environments, in our case, solvents, can result in a modification in the molecular conformation, and these changes can be provoked by the different polarities in the environment. A first summary of these data is shown in Table 1.

**Table 1.** OLEDs main figures of merit properties.

Solvent	Von (V)	Lmax·cd <sup>-2</sup>	η <sub>c</sub> ·cd·A <sup>-1</sup>	η <sub>p</sub> ·lm·W <sup>-1</sup>	EQE <sub>max</sub> %	EQE (@1000·cd m <sup>-2</sup> )%	λ <sub>central</sub> nm	Color Coordinate (x,y)
Toluene	4.0	3270	24.3	16.9	14	9.5	499	0.22, 0.50
THF	5.5	4030	20.0	8.7	10.5	7.9	527	0.28, 0.57
Chlorobenzene	4.5	3060	12.9	8.4	8.2	7.7	498	0.22, 0.47
Chloroform	5.0	2330	3.7	7.9	5.5	4.9	507	0.23, 0.47

A detailed study of the charge-transport mechanisms on these devices was performed. For this purpose, p- and n-type-only devices were made.

Considering the usual SCLC model previously described elsewhere [47,56], we can extract valuable information regarding the electrical parameters involved in the electrical carriers' transport, namely, the N<sub>t</sub> corresponds to the density of traps, E<sub>t</sub> to the energy of traps, μ<sub>h</sub> to the hole mobility, and μ<sub>e</sub> to the electron mobility. Table 2 summarizes these data.

**Table 2.** OLEDs charge-transport properties obtained with the SCLC model and the correspondent EQE for comparison purposes.

Solvent	N <sub>t</sub> (e <sup>-</sup> ) ×10 <sup>17</sup> cm <sup>-3</sup>	N <sub>t</sub> (h <sup>+</sup> ) ×10 <sup>17</sup> cm <sup>-3</sup>	E <sub>t</sub> (e <sup>-</sup> ) mEv	E <sub>t</sub> (h <sup>+</sup> ) mEv	μ <sub>e</sub> ×10 <sup>-12</sup> cm <sup>2</sup> /v.s	μ <sub>h</sub> ×10 <sup>-9</sup> cm <sup>2</sup> /v.s	EQE %
Toluene	5.5	2.5	88.1	46.5	1.0	3.9	14.0
THF	4.6	4.9	61.2	65.8	478.0	5.8	10.5
Chlorobenzene	9.0	8.6	20.0	80.7	9.3	1.9	8.2
Chloroform	6.5	14.8	63.6	82.2	902.0	126	5.5

Looking at Table 2, it is possible to see that the OLED that used THF as solvent for the active layer materials shows the best equilibrium between the mobility of electrons and holes, with this situation being the closest to the ideal one. Ideally, both mobilities should be in the same order of magnitude. In this case, we can consider that the recombination will happen in the middle of the active layer (and considering the p- and n-type organic stack layer thickness). However, if this does not happen and there is a big difference between the mobilities, the recombination can take place outside of the active layer, with further loss of efficiency. This device also has a very good equilibrium for the energy of the traps for both charge carriers. However, the best efficiency was obtained for the OLED with the active layer deposited from a solution with toluene. The best electrical carrier balance will also depend on different factors, particularly the defect densities and their energy levels. Additionally, the charge-transport results also confirm that the OLED that used chloroform as a solvent for the active layer is the worst device. This device shows the best mobility for holes, but there is a difference of three orders of magnitude between the mobility of electrons and holes. Finally, for the OLED that used chlorobenzene for the active layer, the results are, in general, like the ones for toluene. But in this case, high trap densities exist. The energy of the traps for holes is about four times higher than the energy of the traps for electrons.

In the first summary, the data presented in this section show that the solvent used in the active layer will make modifications to the charge-transport mechanisms. These results can be used to explain some differences between the efficiencies for the OLEDs with different solvents, but they also open some questions about these differences that cannot be answered only with these data. These results also show that environmental polarization can be changed by molecular conformity. This one may be changed by the

different types of solvents. Finally, this modification may have originated from triplet-triplet annihilation (TTA).

From a general point of view, different works on solution-deposited OLEDs exhibit very different figures of merit, depending on the emitters (in TADF, it also depends on the  $\Delta E_{ST}$ ), solvents, spin-coating parameters, solvent evaporation, etc. The more representative results show an EQE (the common figure of merit) from 4–6% [57,58] to nearly 15–17% [59,60], with the most common being in the range of 8–12% [61–63]. In this way, the present work appears to be particularly interesting.

### 3.4. Impedance Spectroscopy Characterization

To obtain more insight into differences in the electrical properties observed in the different solution-deposited OLED active layers, the measurements in the AC domain permit a more complete device characterization, giving more details about the different electrical transport (and eventually injection at any interface) properties in the OLED. This part is carried out by evaluating the capacitance, loss, and loss tangent evolution with frequency and the loss evolution with capacitance. Figure 9 shows the plot for capacitance, loss, and loss tangent vs. frequency for all different kinds of devices.

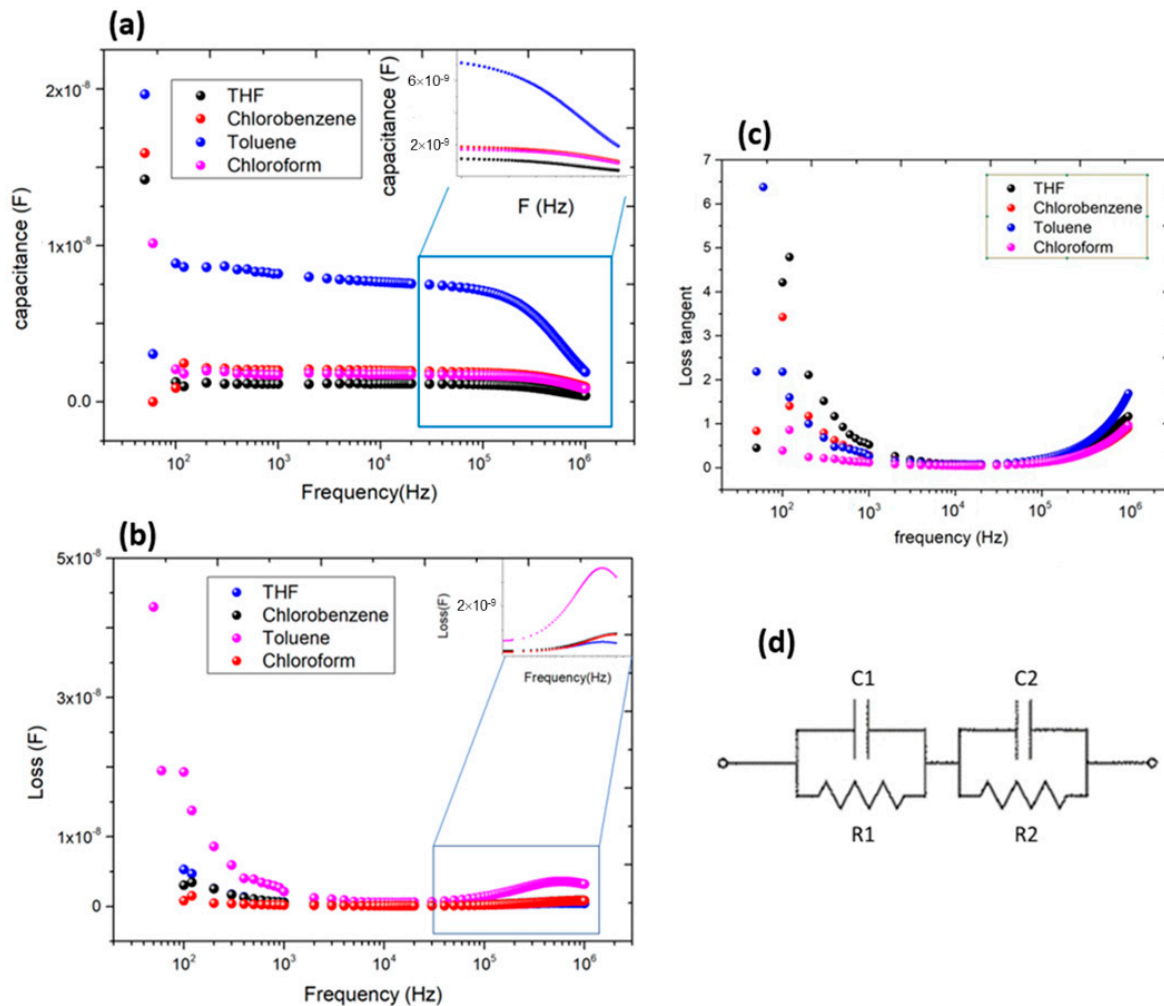


**Figure 9.** Data obtained with the different OLEDs, dependent on the solvents for the active layer: (a) capacitance vs. frequency; (b) loss vs. frequency; (c) loss tangents vs. frequency; (d) equivalent circuit considered for the obtained data analysis.

From the data, it is possible to obtain the Cole–Cole plot that is composed of the loss as a function of the capacitance. Figure 10 is composed of one decreasing part for lower

frequency and a semicircle for medium to high frequency. This figure is typical for a potential barrier with an interface and bulk zone, associating this with the double relaxation process, which is the typical behavior of a double parallel RC. One should be associated with any potential barrier and the other is associated with the semiconductor bulk (due to the differences observed and compared with the OLED figures of merit, this should be in the active layer). However, we cannot exclude different physical processes that can imply more complex equivalent circuits. Therefore, considering the degree of freedom that circuit modulation gives, it is necessary to guarantee that the chosen models represent in the right way the physical processes that happen in the device. In this way, we decided to utilize the simplest solution, the double RC parallel circuit, as seen in Figure 9d. For this circuit, the parallel capacity is given by the following:

$$C_p = C_g + \frac{C_0 - C_g}{1 + (\omega\Gamma)^2}, \quad (1)$$

where

$$C_g = \frac{C_1 C_2}{C_1 + C_2}, \quad C_0 = \frac{C_1 R_1^2 + C_2 R_2^2}{(R_2 + R_1)^2}, \quad \Gamma = \frac{R_2 R_1}{R_1 + R_2} (C_2 + C_1) \quad (2)$$

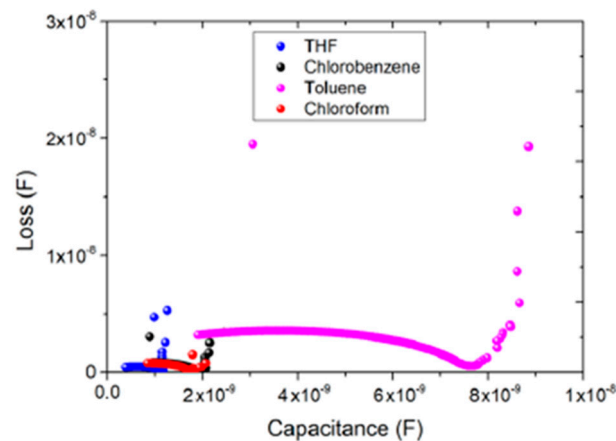


**Figure 10.** Cole–Cole plot for every OLED made with different solvents for the active layer.

The above equations can be easily obtained from the equivalent electrical circuit resolution shown in Figure 9d. It should be noted that the usual series resistance,  $R_s$ , is not represented here and, for all the OLEDs studied, the values are around 1 k $\Omega$ , more specifically changing suitably and assertively with the OLEDs figures of merit.

Analyzing all the AC data, it is observed that for the frequency where the capacity starts to drop, the loss curve and the loss tangent curve start to increase. This drop in the capacity reflects a drop in the charges that can follow the AC signal, and the system starts to lose the capability to polarize. When the loss curve arrives at the maximum point, the loss tangent curve continues to increase and the capacitance curve decreases. This dropping region can have some correspondence in the Cole–Cole plot. The corresponding region is the region where the second relaxation is observed. This is in accordance with the theoretical model that was presented for the double RC circuit that was chosen to be the equivalent circuit that better describes the data obtained.

Looking at the obtained results for the capacity and loss, it is possible to see that the system will have a relaxation for low frequency and another relaxation for high frequency. For the capacitance plot, it is seen that there is a gradual decrease with frequency increase, until nearly 105 Hz. This happens because the frequency is starting to become high, and the charges start to show some resistance to following the AC signal. For this frequency, there is a relaxation peak for every device, but for the OLED that used toluene as solvent for the active layer, this decrease is higher than in the other solvents. The OLED that

used toluene as a solvent for the active layer showed the biggest drop in the capacity value. These drops can be (even indirectly) correlated with the charges' lower mobility because the charge will have more difficulty following the AC signal. In opposition, the devices that used THF and chloroform as solvents for the active layer had a low drop in the capacity value, which can correspond to a lower charge accumulation, making it difficult to follow the AC signal. The OLED where chlorobenzene was used as a solvent for the active layer also had a very low drop. The loss plot also shows a decrease with the frequency increase. But between 104 Hz and 105 Hz, there is an increase in the loss plot until reaching the relaxation peak. In the inset plot of Figure 9a,b, it is possible to see that this peak appears in different frequencies. For toluene, the peak appears near  $5.9 \times 10^5$  Hz, for chlorobenzene near  $6 \times 10^5$  Hz, for chloroform near  $9.9 \times 10^5$  Hz, and for THF at frequencies higher than the ones measured. From the loss tangent plot, the behavior for every solvent is very similar and is in accordance with the theoretical models presented before. The peak for high frequencies corresponds to the point where the capacity starts to decrease. However, there is no visible peak of relaxation. In the Cole–Cole plot, it is again possible to see the double relaxation process. There are remarkable differences among the devices; however, the devices that used chlorobenzene and chloroform for the active layer show the same behavior.

Some correlation between the data obtained and the physical models considered for the equivalent circuit can be carried out. Therefore, examining the model considered for the data analysis, it is possible to see that for low frequencies the equation will go to a constant value that is given by  $C_0$ . That value will have a dependence on the capacitances and resistances. For high frequencies, the equation will go for another constant value,  $C_g$ , that only depends on both capacitances. Both of these constants do not have a frequency dependence. With the association of the experimental data with this model, it is possible to obtain the values for the resistances and capacitances, which can provide more information about the way that charge will flow and will accumulate in the layer.

A full simulation of the equivalent electrical circuit can be performed (numerical convergence methods) to extract the physical data of the circuit. Figure 11 shows such numerical fits.

Looking at these curves, it is possible to see that in every OLED for high frequencies, the model is well adjusted to the experimental data. For the OLED that used chlorobenzene as a solvent for the active layer, at medium frequencies, there is a little discrepancy between the simulated curve and the experimental data. This discrepancy can be related to some physical phenomena that can happen in the device for these frequencies. Also, there exists a discrepancy between the simulated curve and the experimental data at low frequencies. This can be correlated with the equipment limitations at low frequencies.

However, we cannot eliminate the existence of other physical phenomena that can happen in the devices. Table 3 presents the values obtained for the capacitances, resistance, and relaxation times using the equivalent circuit considered for the data analysis and simulations.

With this equivalent circuit, it is possible to consider that, in our case, the first circuit ( $R_1$  and  $C_1$ ) can be related with any interface (although other effects are not out of consideration) and the second circuit ( $R_2$  and  $C_2$ ) can be related with the bulk. In this table, it is possible to see that the OLED that used toluene as solvent for the active layer is the one with the highest  $C_1$  value. Since the capacity is a measure of charge accumulation, this may indicate that, in this OLED, the interface can accumulate more charge than in the other devices. Additionally, this device also shows the highest relaxation time. The OLED that used THF for the active layer was the one that showed the lower value for  $C_1$ . Therefore, if this device has a lower capacity, this can indicate the lower charge accumulated in the interface. The lowest relaxation time for the interface appeared in the OLED that used chlorobenzene for the active layer. This one also showed the second-lowest capacitance. Considering the other RC circuits, it is possible to see that the capacitance values,  $C_2$ , are much lower than the ones for the interface region. Normally, the recombination phenomena happen in this region.

With this, it is expected to have a lower charge accumulation, since most of the charges are recombining. Therefore, if we have high values for the capacity, this can indicate that there is more charge accumulation and, therefore, less recombination. The values for  $C_2$  are very close but there is a little difference for the OLEDs where chloroform and chlorobenzene were used as solvents for the active layer. The OLED that used chlorobenzene for the active layer is the one with lower  $C_2$  values. The lower value can be an indication of the lower charge accumulation and, consequently, more charges for the recombination process. The OLED that used toluene as a solvent for the active layer also has lower  $C_2$  values; this is in accordance with the results for the EQE presented in the previous sections, because in this device there is lower charge accumulation and there are more charges for the recombination process. On the other hand, the OLED that used chloroform as a solvent for the active layer is the one with higher  $C_2$  values. The fact that this value is a little higher than the ones for the other devices can give information about the fact that the charge accumulation is higher and, as a consequence, the charges for the recombination process will be lower. The second relaxation time presented in the table corresponds to the relaxation that appears for higher frequencies in the capacitance and loss plots. These relaxation phenomena can be related to the physical properties of the active layer.

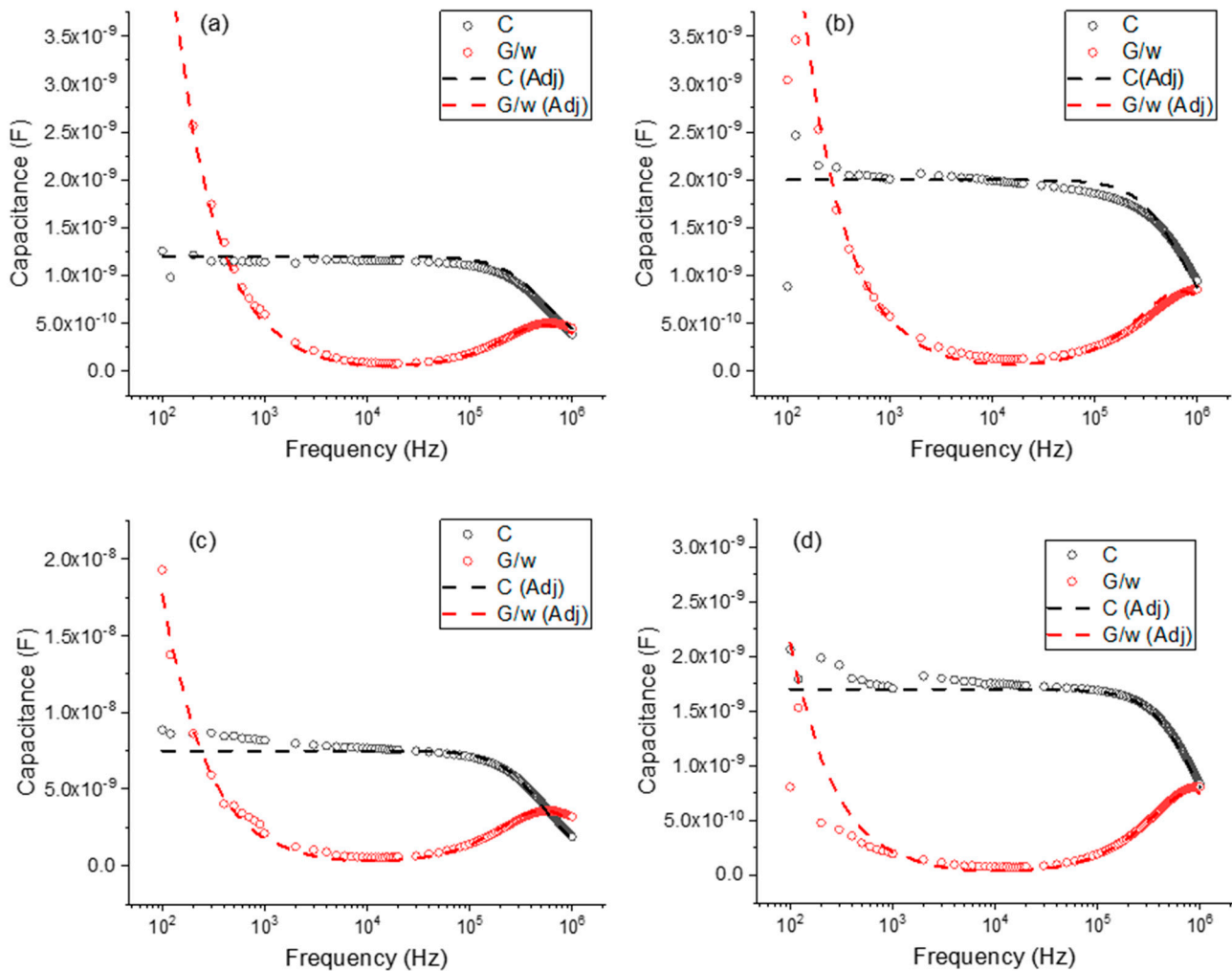


**Figure 11.** Capacitance (C) and loss ( $G/\omega$ ) data for the different kinds of OLEDs fabricated. Open circles: experimental data; lines: fitting using the double RC circuit. (a) THF as solvent, (b) chlorobenzene as solvent, (c) toluene as solvent, and (d) chloroform as solvent.

**Table 3.** Values obtained with the fittings for the equivalent circuit resistances and capacitances, and the respective times of relaxation.

Solvent	$R_1$ (K $\Omega$ )	$C_1$ (nF)	$\tau_1$ (ms)	$R_2$ ( $\Omega$ )	$C_2$ (nF)	$\tau_2$ (ns)
Toluene	90	7.5	0.675	40	0.3	12
THF	320	1.2	0.384	200	0.3	60
Chlorobenzene	750	1.7	0.128	100	0.2	20
Chloroform	300	2.0	0.600	95	0.4	30

The existence of traps in the devices implies that there exists a finite time for the charge interaction with electrically active levels (some certainly arising from defects). Therefore, the device with a lower relaxation time is the one that used toluene for the active layer, and the device with a higher relaxation time, for the high-frequency relaxation, is the one that used THF as solvent for the active layer. Considering these results, it is possible to assume that in the OLED that used toluene for the active layer, the charge interaction with the traps is possibly lower than in the other devices.

In summary, with every consideration made, it is possible to conclude that the solvent will induce changes in the molecular conformation. If we look at the guest: host energy transfer process, the photophysical data indicate that the solvent will not induce changes, and, therefore, the electrical charge transport and accumulation need to be the fundamental explanation for the differences obtained. Finally, considering the impedance spectroscopy, it is possible to conclude that differences in the charge accumulation and in the interaction time between the charges and the trap levels are consequences of the different molecular conformation at the active layer because of the different solution properties employed in the deposition. Therefore, a correct choice of solvent appears to be one way to further exploration.

#### 4. Conclusions

This work aimed to develop and characterize OLEDs based on a 2PXZ-OXD green TADF, in simplified structures (two organic layers), and their optimization. Solution-deposited OLEDs are particularly prone to producing organic layers with a high density of intrinsic defects that negatively impact the device's performance. Here, we tried to optimize the OLED active layer deposited using different solvents and tentatively establish an electrical model that can explain the different results. The focus was on achieving the best trade-off between device performance and structure optimization with the best possible molecular conformation. The work involved the wet manufacturing of OLEDs (spin-coating) and the electro-optical characterization, giving the figures of merit based on the applicable physical models for the injection/transport and recombination of electrical charge.

From the analysis of the figures of merit, we can conclude that the best device was the one that used toluene as a solvent for the active layer, with figures of merit near the best reported in the literature but with a more complex device structure. This maximum brightness was 3240 cd.m<sup>-2</sup>,  $\eta_{c,max}$  of 24.3 cd.A<sup>-1</sup>,  $\eta_{p,max}$  of 16.9 lm.W<sup>-1</sup>, and a maximum EQE of 14%. On the other hand, the worst device was the one that used chloroform as solvent. By using DC electrical characterization, it was possible to correlate the data with intrinsic defect formation and electrical balance of the carriers inside the active layer.

By using impedance spectroscopy, we conclude that the system can be modulated by two RC parallel circuits in series. The capacitance vs. frequency plot shows differences for the four types of OLEDs; one factor that can explain these differences is the charge mobility in the device. With the numerical data fitting, it was possible to obtain the parameters to describe the equivalent circuit. A relationship between relaxation times and pure figures of merit can be obtained, helping to provide a better understanding of the molecular conformation differences in the OLED active layer, and opening new opportunities for further developments.

**Author Contributions:** Conceptualization, L.P.; methodology, F.T., J.C.G. and L.P.; software, L.P.; validation, F.T., J.C.G. and L.P.; formal analysis, F.T., J.C.G. and L.P.; investigation, F.T., J.C.G. and L.P.; resources, L.P.; data curation, writing—original draft preparation, F.T., J.C.G. and L.P.; writing—review and editing, J.C.G. and L.P.; visualization, F.T., J.C.G. and L.P.; supervision, J.C.G. and L.P.; project administration, L.P.; funding acquisition, L.P. All authors have read and agreed to the published version of the manuscript.

**Funding:** F.M.T., J.C.G. and L.P. acknowledge the Institute for Nanostructures, Nanomodelling and Nanofabrication (i3N), Portuguese Foundation for Science and Technology (FCT) (UIDB/50025/2020 and UIDP/50025/2020). J.C.G. also thanks FCT/i3N/UA for the individual CEEC grant (2021.02056.CEECIND).

**Institutional Review Board Statement:** Not applicable.

**Informed Consent Statement:** Not applicable.

**Data Availability Statement:** Data are available upon reasonable request.

**Conflicts of Interest:** The authors declare no conflict of interest.

## References

1. Tang, C.W.; Vanslyke, S.A. Organic Electroluminescent Diodes. *Appl. Phys. Lett.* **1987**, *51*, 913–915. [[CrossRef](#)]
2. Hong, G.; Gan, X.; Leonhardt, C.; Zhang, Z.; Seibert, J.; Busch, J.M.; Bräse, S. A Brief History of OLEDs—Emitter Development and Industry Milestones. *Adv. Mater.* **2021**, *33*, e2005630. [[CrossRef](#)] [[PubMed](#)]
3. Minotto, A.; Bulut, I.; Rapidis, A.G.; Carnicella, G.; Patrini, M.; Lunedei, E.; Anderson, H.L.; Cacialli, F. Towards Efficient Near-Infrared Fluorescent Organic Light-Emitting Diodes. *Light Sci. Appl.* **2021**, *10*, 18. [[CrossRef](#)] [[PubMed](#)]
4. Shin, H.; Lee, J.-H.; Moon, C.-K.; Huh, J.-S.; Sim, B.; Kim, J.-J. Sky-Blue Phosphorescent OLEDs with 34.1% External Quantum Efficiency Using a Low Refractive Index Electron Transporting Layer. *Adv. Mater.* **2016**, *28*, 4920–4925. [[CrossRef](#)] [[PubMed](#)]
5. Wong, M.Y.; Zysman-Colman, E. Purely Organic Thermally Activated Delayed Fluorescence Materials for Organic Light-Emitting Diodes. *Adv. Mater.* **2017**, *29*, 1605444. [[CrossRef](#)] [[PubMed](#)]
6. Liu, D.; Tian, W.; Feng, Y.; Zhang, X.; Ban, X.; Jiang, W.; Sun, Y. Achieving 20% External Quantum Efficiency for Fully Solution-Processed Organic Light-Emitting Diodes Based on Thermally Activated Delayed Fluorescence Dendrimers with Flexible Chains. *ACS Appl. Mater. Interfaces* **2019**, *11*, 16737–16748. [[CrossRef](#)] [[PubMed](#)]
7. Li, C.; Xu, Y.; Liu, Y.; Ren, Z.; Ma, Y.; Yan, S. Highly Efficient White-Emitting Thermally Activated Delayed Fluorescence Polymers: Synthesis, Non-Doped White OLEDs and Electroluminescent Mechanism. *Nano Energy* **2019**, *65*, 104057. [[CrossRef](#)]
8. Liu, H.; Fu, Y.; Chen, J.; Tang, B.Z.; Zhao, Z. Energy-Efficient Stable Hyperfluorescence Organic Light-Emitting Diodes with Improved Color Purities and Ultrahigh Power Efficiencies Based on Low-Polar Sensitizing Systems. *Adv. Mater.* **2023**, *35*, e2212237. [[CrossRef](#)]
9. Bian, M.; Zhang, D.; Wang, Y.; Chung, Y.-H.; Liu, Y.; Ting, H.; Duan, L.; Chen, Z.; Bian, Z.; Liu, Z.; et al. Long-Lived and Highly Efficient TADF-PhOLED with “(A) n –D–(A) n” Structured Terpyridine Electron-Transporting Material. *Adv. Funct. Mater.* **2018**, *28*, 1800429. [[CrossRef](#)]
10. Sun, J.W.; Lee, J.-H.; Moon, C.-K.; Kim, K.-H.; Shin, H.; Kim, J.-J. A Fluorescent Organic Light-Emitting Diode with 30% External Quantum Efficiency. *Adv. Mater.* **2014**, *26*, 5684–5688. [[CrossRef](#)]
11. Ban, X.; Chen, F.; Pan, J.; Liu, Y.; Zhu, A.; Jiang, W.; Sun, Y. Exciplex Formation and Electromer Blocking for Highly Efficient Blue Thermally Activated Delayed Fluorescence OLEDs with All-Solution-Processed Organic Layers. *Chem. Eur. J.* **2020**, *26*, 3090–3102. [[CrossRef](#)] [[PubMed](#)]
12. Tian, Q.S.; Shen, W.S.; Yu, Y.J.; Wang, X.Q.; Cai, J.H.; Hu, Y.; Jiang, Z.Q.; Huang, J.S.; Liao, L.S. Systematic Strategy for High-Performance Small Molecular Hybrid White OLED via Blade Coating at Ambient Condition. *Org. Electron.* **2022**, *100*, 106366. [[CrossRef](#)]
13. Kant, C.; Mahmood, S.; Katiyar, M. Large-Area Inkjet-Printed OLEDs Patterns and Tiles Using Small Molecule Phosphorescent Dopant. *Adv. Mater. Technol.* **2023**, *8*, 2201514. [[CrossRef](#)]
14. Amruth, C.; Dubey, D.K.; Pahlevani, M.; Welch, G.C. Slot-Die Coating of All Organic/Polymer Layers for Large-Area Flexible OLEDs: Improved Device Performance with Interlayer Modification. *Adv. Mater. Technol.* **2021**, *6*, 2100264. [[CrossRef](#)]
15. Guo, K.; Tang, Z.; Chou, X.; Pan, S.; Wan, C.; Xue, T.; Ding, L.; Wang, X.; Huang, J.; Zhang, F.; et al. Printable Organic Light-Emitting Diodes for next-Generation Visible Light Communications: A Review. *Adv. Photon. Nexus* **2023**, *2*, 044001. [[CrossRef](#)]
16. Kim, H.J.; Godumala, M.; Kim, S.K.; Yoon, J.; Kim, C.Y.; Park, H.; Kwon, J.H.; Cho, M.J.; Choi, D.H. Color-Tunable Boron-Based Emitters Exhibiting Aggregation-Induced Emission and Thermally Activated Delayed Fluorescence for Efficient Solution-Processable Nondoped Deep-Blue to Sky-Blue OLEDs. *Adv. Opt. Mater.* **2020**, *8*, 1902175. [[CrossRef](#)]
17. Cariati, E.; Lucenti, E.; Botta, C.; Giovanella, U.; Marinotto, D.; Righetto, S. Cu(I) Hybrid Inorganic–Organic Materials with Intriguing Stimuli Responsive and Optoelectronic Properties. *Coord. Chem. Rev.* **2015**, *306*, 566–614. [[CrossRef](#)]

18. Liang, X.; Tu, Z.L.; Zheng, Y.X. Thermally Activated Delayed Fluorescence Materials: Towards Realization of High Efficiency through Strategic Small Molecular Design. *Chem. A Eur. J.* **2019**, *25*, 5623–5642. [[CrossRef](#)]
19. Naveen, K.R.; Yang, H.I.; Kwon, J.H. Double Boron-Embedded Multiresonant Thermally Activated Delayed Fluorescent Materials for Organic Light-Emitting Diodes. *Commun. Chem.* **2022**, *5*, 149. [[CrossRef](#)]
20. Yuan, W.; Hu, D.; Zhu, M.; Shi, W.; Shi, C.; Sun, N.; Tao, Y. Simple Peripheral Modification for Color Tuning of Thermally Activated Delayed Fluorescence Emitters in OLEDs. *Dye. Pigment.* **2021**, *191*, 109395. [[CrossRef](#)]
21. Naveen, K.R.; Palanisamy, P.; Chae, M.Y.; Kwon, J.H. Multiresonant TADF Materials: Triggering the Reverse Intersystem Crossing to Alleviate the Efficiency Roll-off in OLEDs. *Chem. Commun.* **2023**, *59*, 3685–3702. [[CrossRef](#)] [[PubMed](#)]
22. Fan, X.; Hao, X.; Huang, F.; Yu, J.; Wang, K.; Zhang, X. RGB Thermally Activated Delayed Fluorescence Emitters for Organic Light-Emitting Diodes toward Realizing the BT.2020 Standard. *Adv. Sci.* **2023**, *10*, 2303504. [[CrossRef](#)] [[PubMed](#)]
23. Wang, D.; Zhang, Q. Fundamental Theories of TADF. In *Thermally Activated Delayed Fluorescence Organic Light-Emitting Diodes (TADF-OLEDs)*; Elsevier: Amsterdam, The Netherlands, 2022; pp. 71–89. [[CrossRef](#)]
24. Manish, K.; Miguel, R.; Luiz, P. New generation of high efficient OLED using Thermally Activated Delayed Fluorescent materials. In *Light-Emitting Diode: An Outlook on the Empirical Features and Its Recent Technological Advancements*; InTech Open: London, UK, 2018; ISBN 978-953-51-5972-8.
25. Northey, T.; Stacey, J.; Penfold, T.J. The Role of Solid State Solvation on the Charge Transfer State of a Thermally Activated Delayed Fluorescence Emitter. *J. Mater. Chem. C* **2017**, *5*, 11001–11009. [[CrossRef](#)]
26. Phan Huu, D.K.A.; Saseendran, S.; Dhali, R.; Franca, L.G.; Stavrou, K.; Monkman, A.; Painelli, A. Thermally Activated Delayed Fluorescence: Polarity, Rigidity, and Disorder in Condensed Phases. *J. Am. Chem. Soc.* **2022**, *144*, 15211–15222. [[CrossRef](#)] [[PubMed](#)]
27. Li, F.; Li, M.; Fan, J.; Song, Y.; Wang, C.K.; Lin, L. Theoretical Study on Thermally Activated Delayed Fluorescence Emitters in White Organic Light-Emitting Diodes: Emission Mechanism and Molecular Design. *J. Phys. Chem. A* **2020**, *124*, 7526–7537. [[CrossRef](#)]
28. Schleper, A.L.; Goushi, K.; Bannwarth, C.; Haehnle, B.; Welscher, P.J.; Adachi, C.; Kuehne, A.J.C. Hot Exciplexes in U-Shaped TADF Molecules with Emission from Locally Excited States. *Nat. Commun.* **2021**, *12*, 6179. [[CrossRef](#)]
29. Monkman, A. Photophysics of Thermally Activated Delayed Fluorescence. In *Highly Efficient OLEDs: Materials Based on Thermally Activated Delayed Fluorescence*; Wiley-VCH: Weinheim, Germany, 2018; pp. 425–463. [[CrossRef](#)]
30. Eng, J.; Penfold, T.J. Open Questions on the Photophysics of Thermally Activated Delayed Fluorescence. *Commun. Chem.* **2021**, *4*, 21–24. [[CrossRef](#)]
31. Eng, J.; Penfold, T.J. Understanding and Designing Thermally Activated Delayed Fluorescence Emitters: Beyond the Energy Gap Approximation. *Chem. Rec.* **2020**, *20*, 831–856. [[CrossRef](#)]
32. Abbel, R.; de Vries, I.; Langen, A.; Kirchner, G.; t'Mannetje, H.; Gorter, H.; Wilson, J.; Groen, P. Toward high volume solution based roll-to-roll processing of OLEDs. *J. Mater. Res.* **2017**, *32*, 2219–2229. [[CrossRef](#)]
33. Fatemeh Samaeifar, F.; Aziz, H. Role of Guest Materials in the Lower Stability of Solution-Coated versus Vacuum-Deposited Phosphorescent OLEDs. *ACS Appl. Mater. Interfaces* **2022**, *14*, 8199–8208. [[CrossRef](#)]
34. Sanderson, S.; Vamvounis, G.; Mark, A.E.; Burn, P.L.; White, R.D.; Philippa, B.W. Understanding the performance differences between solution and vacuum deposited OLEDs: A computational approach. *J. Chem. Phys.* **2022**, *156*, 214703. [[CrossRef](#)] [[PubMed](#)]
35. Shibata, M.; Sakaib, Y.; Yokoyama, D. Advantages and disadvantages of vacuum-deposited and spin-coated amorphous organic semiconductor films for organic light-emitting diodes. *J. Mater. Chem. C* **2015**, *3*, 11178. [[CrossRef](#)]
36. Han, T.-H.; Choi, M.-R.; Jeon, C.-W.; Kim, Y.-H.; Kwon, S.-K.; Lee, T.-W. Ultrahigh-efficiency solution-processed simplified small-molecule organic light-emitting diodes using universal host materials. *Sci. Adv.* **2016**, *2*, e160142. [[CrossRef](#)] [[PubMed](#)]
37. Guo, F.; Karl, A.; Xue, Q.-F.; Tam, K.C.; Forberich, K.; Brabec, C.J. The fabrication of color-tunable organic light-emitting diode displays via solution processing. *Light Sci. Appl.* **2017**, *6*, e17094. [[CrossRef](#)]
38. Zhang, M.; Höfle, S.; Czolk, S.; Mertens, A.; Colmann, A. All-solution processed transparent organic light emitting diodes. *Nanoscale* **2015**, *7*, 20009. [[CrossRef](#)] [[PubMed](#)]
39. Wei, J.; Liu, D.; Sun, K.; Tian, W.; Jiang, W.; Sun, Y. Enhanced performances of fully solution-processed OLEDs via introducing flexible chains into thermally cross-linked thermally activated delayed fluorescent materials. *Dye. Pigment.* **2020**, *182*, 108624. [[CrossRef](#)]
40. Woo, J.Y.; Park, M.-H.; Jeong, S.-H.; Kim, Y.-H.; Kim, B.; Lee, T.-W.; Han, T.-H. Advances in Solution-Processed OLEDs and their Prospects for Use in Displays. In *Advanced Materials*; Wiley Online Library: Hoboken, NJ, USA, 2023; p. 2207454.
41. Perumal, A.; Faber, H.; Yaacobi-Gross, N.; Pattanasattayavong, P.; Burgess, C.; Jha, S.; McLachlan, M.A.; Stavrinou, P.N.; Anthopoulos, T.D.; Bradley, D.D.C. High-Efficiency, Solution-Processed, Multilayer Phosphorescent Organic Light-Emitting Diodes with a Copper Thiocyanate Hole-Injection/Hole-Transport Layer. *Adv. Mater.* **2015**, *27*, 93–100. [[CrossRef](#)]
42. Lin, T.; Sun, X.; Hu, Y.; Mu, W.; Sun, Y.; Zhang, D.; Su, Z.; Chu, B.; Cui, Z. Blended host ink for solution processing high performance phosphorescent OLEDs. *Sci. Rep.* **2019**, *9*, 6845. [[CrossRef](#)]
43. Samaeifar, F.; Aziz, H. The Root Causes of the Limited Electroluminescence Stability of Solution-Coated Versus Vacuum-Deposited Small-Molecule OLEDs: A Mini-Review. *Front. Chem.* **2022**, *10*, 857551. [[CrossRef](#)]

44. Kumar, M.; Chapran, M.; Wiosna-Sałyga, G.; Sleczkowski, P.; Luszczynska, B.; Pereira, L. An Insight on Charge Transport in High Efficient Green Solution-Processed TADF OLEDs with a Single Emitting Layer. *J. Phys. Chem. C* **2020**, *124*, 21935–21947. [[CrossRef](#)]
45. Kumar, M.; Pereira, L. Mixed-Host Systems with a Simple Device Structure for Efficient Solution-Processed Organic Light-Emitting Diodes of a Red-Orange TADF Emitter. *ACS Omega* **2020**, *5*, 2196–2204. [[CrossRef](#)] [[PubMed](#)]
46. Kumar, M.; Pereira, L. Towards Highly Efficient TADF Yellow-Red OLEDs Fabricated by Solution Deposition Methods: Critical Influence of the Active Layer. *Nanomaterials* **2020**, *10*, 101. [[CrossRef](#)] [[PubMed](#)]
47. Pereira, L. *Organic Light Emitting Diodes: The Use of Rare Earth and Transition Metals*; CRC Press: Singapore, 2012.
48. Manish, K.; Luiz, P. Development of Efficient OLEDs from Solution Deposition. *J. Vis. Exp.* **2022**, *189*, e61071. [[CrossRef](#)]
49. Bonon, B.M.A.; Atvars, T.D.Z. Energy transfer from poly(vinyl carbazole) to a fluorenevinylene copolymer in solution and in the solid state. *Photochem. Photobiol.* **2012**, *88*, 801–809. [[CrossRef](#)]
50. Germino, J.C.; Duarte, L.G.T.A. Photophysics basic concepts. In *Semiconducting Polymers: Synthesis and Photophysical Properties*, 1st ed.; Apple Academic Press: Cambridge, MA, USA, 2021; Volume 1, pp. 39–72.
51. Germino, J.C.; de Freitas, J.N.; Domingues, R.A.; Quides, F.J.; Faleiros, M.M.; Atvars, T.D.Z. Organic light-emitting diodes based on PVK and Zn(II) salicylidene composites. *Synth. Met.* **2018**, *241*, 7–16. [[CrossRef](#)]
52. Lee, J.; Shizu, K.; Tanaka, H.; Nomura, H.; Yasuda, T.; Adachi, C. Oxadiazole- and Triazole-Based Highly-Efficient Thermally Activated Delayed Fluorescence Emitters for Organic Light-Emitting Diodes. *J. Mater. Chem. C* **2013**, *1*, 4599–4604. [[CrossRef](#)]
53. Knyazev, A.A.; Krupin, A.S.; Romanova, K.A.; Galyametdinov, Y.G. Luminescence and Energy Transfer in Poly(N-Vinylcarbazole) Blends Doped by a Highly Anisometric Eu(III) Complex. *J. Coord. Chem.* **2016**, *69*, 1473–1483. [[CrossRef](#)]
54. Rodríguez-Mas, F.; Ferrer, J.C.; Alonso, J.L.; de Fernández Ávila, S.; Valiente, D. Reduced Graphene Oxide Inserted into PEDOT:PSS Layer to Enhance the Electrical Behaviour of Light-Emitting Diodes. *Nanomaterials* **2021**, *11*, 645. [[CrossRef](#)]
55. NIST. Oxazole. Available online: <https://webbook.nist.gov/cgi/cbook.cgi?ID=C288426&Mask=80,9> (accessed on 22 September 2022).
56. Lampert, M.A.; Mark, P. *Current Injection in Solids*; Academic Press: New York, NY, USA, 1970.
57. Joo, C.W.; Cho, H.; Kwon, B.-H.; Cho, N.S.; Kim, Y.; Kim, Y.-H.; Lee, J. Development of solution-processable blue/hybrid-white OLEDs based on thermally activated delayed fluorescence. *J. Ind. Eng. Chem.* **2018**, *65*, 35–39. [[CrossRef](#)]
58. Albrecht, K.; Matsuoka, K.; Yokoyama, D.; Sakai, Y.; Nakayama, A.; Fujita, K.; Yamamoto, K. Thermally activated delayed fluorescence OLEDs with fully solution processed organic layers exhibiting nearly 10% external quantum efficiency. *Chem. Commun.* **2017**, *53*, 2439–2442. [[CrossRef](#)]
59. Ban, X.; Zhu, A.; Zhang, T.; Tong, Z.; Jiang, W.; Sun, Y. Highly Efficient All-Solution-Processed Fluorescent Organic Light-Emitting Diodes Based on a Novel Self-Host Thermally Activated Delayed Fluorescence Emitter. *ACS Appl. Mater. Interfaces* **2017**, *9*, 21900–21908. [[CrossRef](#)]
60. Albrecht, K.; Matsuoka, K.; Fujita, K.; Yamamoto, K. A dendrimer emitter doped in a dendrimer host: Efficient thermally activated delayed fluorescence OLEDs with fully-solution processed organic-layers. *Mater. Chem. Front.* **2018**, *2*, 1097–1103. [[CrossRef](#)]
61. Lee, S.Y.; Yasuda, T.; Komiyama, H.; Lee, J.; Adachi, C. Thermally Activated Delayed Fluorescence Polymers for Efficient Solution-Processed Organic Light-Emitting Diodes. *Adv. Mat.* **2016**, *28*, 4019–4024. [[CrossRef](#)] [[PubMed](#)]
62. Li, W.; Zhao, J.; Li, L.; Du, X.; Fan, C.; Zheng, C.; Tao, S. Efficient solution-processed blue and white OLEDs based on a high-triplet bipolar host and a blue TADF emitter. *Org. Electr.* **2018**, *58*, 276–282. [[CrossRef](#)]
63. Li, Y.; Xie, G.; Gong, S.; Wu, K.; Yang, C. Dendronized delayed fluorescence emitters for non-doped, solution-processed organic light-emitting diodes with high efficiency and low efficiency roll-off simultaneously: Two parallel emissive channels. *Chem. Sci.* **2016**, *7*, 5441–5447. [[CrossRef](#)]

**Disclaimer/Publisher’s Note:** The statements, opinions and data contained in all publications are solely those of the individual author(s) and contributor(s) and not of MDPI and/or the editor(s). MDPI and/or the editor(s) disclaim responsibility for any injury to people or property resulting from any ideas, methods, instructions or products referred to in the content.